

# Many-Objective Simulation-Based Optimization of an Air Separation Unit

Santiago D. Salas\* Dany De Cecchis\* Bryan V. Piguave\*  
José A. Romagnoli\*\*

\* *Escuela Superior Politécnica del Litoral, ESPOL, Facultad de Ciencias Naturales y Matemáticas, Campus Gustavo Galindo Km. 30.5 Vía Perimetral, P.O. Box 09-01-5863, Guayaquil, Ecuador.*

\*\* *Department of Chemical Engineering, Louisiana State University, Baton Rouge, LA 70803, United States.*

---

**Abstract:** Air separation systems are crucial in the production of oxygen, which has gained particular relevance during the COVID-19 outbreak. Mechanical ventilation can compensate respiratory deficiencies along with the use of medical oxygen in vulnerable patients infected with this disease. In this contribution, a many-objective simulation-based optimization framework is proposed for determining eleven decision variables for the operation of an air separation unit. The framework combines the capabilities of the process simulator PRO/II with a Python environment. Three objective functions are optimized together towards the construction of a 3-D Pareto front. Results provide insightful information regarding the most adequate operating conditions of the unit, including the definition of an operational window rather than a single operational point.

*Keywords:* Many-objective optimization, 3-D Pareto front, Cryogenic air distillation, Operational window.

---

## 1. INTRODUCTION

Governments and the healthcare sector worldwide have struggled during the COVID-19 outbreak in 2020. At the peak of infected cases some cities have experienced the scarcity of oxygen supply. Medical oxygen is prescribed to patients through mechanically ventilated devices at the intensive care units aiming for the patient's recovery (Whittle et al., 2020). In this context, this infectious disease has risen the attention towards oxygen supply facilities. A cryogenic air separation unit (ASU) is employed to separate air into its principal constituents, primarily oxygen (O<sub>2</sub>), nitrogen (N<sub>2</sub>) and argon (Ar). However, these products might vary in their purity, phase and produced quantities.

ASUs are well studied systems that usually consist of three sections: compression, refrigeration, and separation. In this context, Zhu et al. (2001) implemented a low-order dynamic model for a cryogenic distillation column utilized mainly for N<sub>2</sub> purification using the process simulator HYSYS. Jiang et al. (2003) examined the optimization of a pressure-swing absorption (PSA) system for air separation tailoring optimization algorithms. Huang et al. (2009) proposed a nonlinear model predictive control for adjusting the operating conditions of a PSA system and for responding to variations in the product demand. Searching for design improvements, Manenti et al. (2013) studied the process intensification of an ASU using the commercial simulator PRO/II. The main aims in this work were to

improve the O<sub>2</sub> purity, the recycle of the rich Ar stream and to evaluate the feasibility of producing energy. Aneke and Wang (2015) analyzed the implementation of heat recovery cycles with different configurations at the compression stage for enhancing the energy efficiency of the system. Negrellos-Ortiz et al. (2018) studied the dynamic optimization of a cryogenic ASU using a derivative-free optimization strategy and the simulation package ASPEN Dynamics. Regarding improvements in the compression stage, Tesch et al. (2017) evaluated the integration of LNG regasification into air separation processes. In this case, an exergy and an economic analysis were carried out using the process simulator ASPEN Plus. Even though the aforementioned contributions have addressed simulation-based approaches, the utilization of many-objective optimizations has not been reported in the literature. The advantage of these optimization strategies is that the set of Pareto-optimal points permits to define operational windows based on the resultant decision variables.

In this contribution, a simulation-based many-objective optimization approach is proposed for determining eleven key decision variables of an ASU while optimizing three conflicting objectives. The simulation model incorporates a compression train located upstream the ASU. In our practice, the process simulator PRO/II and a Python environment are integrated following the guidelines introduced by Jones et al. (2019). Herein, the three objective functions are the annualized cash flow (*CF*), the efficiency of the Rankine Cycle at the compression stage (*ef*), and the capital expenditures (*CAPEX*) of the facility. The first two objectives are maximized while the third objective

---

\* This work is part of the project FCNM-54-2020 registered at ESPOL, and jointly supported by PSE@LSU and PSE@ESPOL.

is minimized using a high-level evolutionary optimization algorithm for many-objective problem formulations known as the reference vector-guided evolutionary algorithm (RVEA) (Cheng et al., 2016). The achieved results provide guidance regarding the most adequate operating conditions of the integrated system in which an operational window for each decision variable is determined based on a 3-D Pareto front.

## 2. ASU PROCESS DESCRIPTION

The production of oxygen starts with a pre-treatment stage. In this section all the impurities, including carbon dioxide and water, are removed for avoiding operational inconveniences, such as the formation of hydrates downstream the process. This stage is typically carried out using molecular sieve adsorbers (Castle, 2002).

Thereafter, the pressure of the air stream increases to 607.95 kPa. To achieve this condition, three compressors arranged in series, are incorporated (C-101/102/103). An average compression ratio of 2:1 is set for each unit. The outlet temperature of the process stream is maintained in approximately 295 K by the heat exchangers (E-101/102/103). In this contribution, a recovery Rankine cycle is implemented for converting the adsorbed heat, generated by the compression of air, into electricity. The assumed efficiency of the equipment in this section is 80%. The proposed arrangement aims to reduce the energy consumption of the facility while promoting an efficient operation of the system (Singla and Chowdhury, 2019).

The compressed air is split into two streams. In this sense, 10% is sent to the compressor C-201 and the remainder to the multi-stream heat exchanger E-201. After the heat exchange occurs, the first stream enters to the expander C-202 and reduces its pressure to 150 kPa. The produced energy due to the pressure drop is used by the compressor C-201 considering a 90% efficiency of the expander.

The top pressure of the high-pressure column (T-201) is set at 600 kPa. A concentration of 35% of  $O_2$  is obtained in the stream at the bottoms of this column. Regarding the design of the column, a total condenser is considered. The overhead stream is directed to the low-pressure column (T-202) which operates at 150 kPa. This stream works as the reflux of the column T-202. The selected arrangement benefits the relative volatility between  $O_2$  and  $N_2$  in the unit. As part of the heat integration process, the overhead stream of the column T-202, which corresponds to the produced  $N_2$ , enters to the multi-stream heat exchanger E-202 and then to the E-201. Moreover, the product obtained in the bottoms stream of the T-202 has an  $O_2$  concentration above 99%. The residual Ar is removed by the side column T-203 which has a condenser that operates at 150 kPa. This column receives the bottoms product of the T-201 and a stream derived from the stage 44 of the column T-202.

The process flow diagram of the system is illustrated in Figure 1. This diagram includes the compression section and the ASU. The system is simulated using the commercial process simulator PRO/II in steady-state. The high-resolution model incorporates quality constraints to ensure that the products comply with desired quality

standards such as the degree of purity. In addition, to simulate and calculate the multi-stream exchanger E-202, two units were required as well as the incorporation of reference streams. The path of each flow stream is traceable within the process, facilitating further analyses. Finally, the pseudo-streams on each distillation column permit to incorporate the energy integration of the whole heat exchange network.

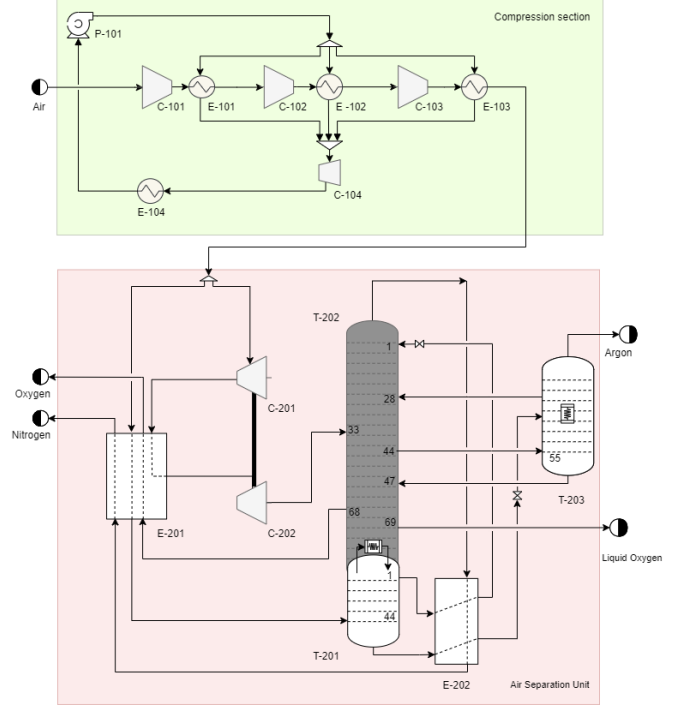


Fig. 1. Process flow diagram of the air separation unit including the compression system.

## 3. MANY-OBJECTIVE OPTIMIZATION FRAMEWORK

### 3.1 Optimization formulation

In this work, three objective functions are considered. The first two objectives are maximized  $f_1(x)$  and  $f_2(x)$ , while the third objective  $f_3(x)$  is minimized. We define the optimization problem as

$$\max_x [f_1(x), f_2(x)], \min_x f_3(x), \quad (1)$$

subject to

$$\begin{aligned} h(x) &= 0, \\ g(x) &\leq 0, \\ x^{LB} &\leq x \leq x^{UB}, \end{aligned}$$

where, the equality constraints are denoted by  $h(x)$  and are intrinsically included in the process simulation. The inequality constraints correspond to  $g(x)$  and are taken into account when verifying the convergence of the simulation as well as design constraints.  $x \in \mathbb{R}^{11}$  is the vector of decision variables constrained between lower and upper bounds.

The first objective function  $f_1(x)$  is the  $CF(x)$ , which is calculated by subtracting the operational expenditures

( $OPEX(x)$ ) of the process from the generated revenues, this is defined by

$$f_1(x) \equiv CF(x) = \sum_{i=1}^P c_i F_i(x) - OPEX(x). \quad (2)$$

The revenues are calculated summing the product between the price,  $c_i$ , and the flow rate,  $F_i(x)$ , of each produced air constituent  $i = 1, \dots, P$ . In this case, we consider three air constituents,  $O_2$ ,  $N_2$  and  $Ar$ , i.e.  $P = 3$ . The  $OPEX(x)$  is defined below in Eq. (5).

The efficiency  $ef(x)$  at the compression stage of the ASU is the second objective function  $f_2(x)$ . The  $ef(x)$  is the ratio between the work generated by the expander,  $W_{exp}(x)$ , and the sum of the heat removed by the heat exchangers at the compression,  $Q_{hex,j}(x)$ , with  $j = 1, 2, \dots, q$ , in this case  $q = 3$ . A generic equation is defined next

$$f_2(x) \equiv ef(x) = \frac{W_{exp}(x)}{\sum_{j=1}^q Q_{hex,j}(x)}. \quad (3)$$

Finally, the  $CAPEX(x)$  corresponds to the third objective function and denotes the capital investment required for the facility. The  $CAPEX(x)$  is calculated by summing the cost bare module ( $C_{BM}(x)$ ) of each rotatory and static equipment  $e$ . The total summation is multiplied by 1.18 times the ratio between the chemical engineering plant cost index ( $CEPCI$ ) of 2019 and a base year (2001), producing the following expression

$$f_3(x) \equiv CAPEX(x) = 1.18 \left( \sum_{e=1}^E C_{BM,e}(x) \right) \frac{CEPCI_{2019}}{CEPCI_{base}}. \quad (4)$$

The  $OPEX(x)$ , used in Eq. (2), considers the 18% of the  $CAPEX(x)$ , the raw material costs ( $RMC$ ) and the utility cost ( $UC(x)$ ), this is

$$OPEX(x) = 0.18 CAPEX(x) + 1.23 (RMC + UC(x)). \quad (5)$$

The prices of the products as well as the cost of air conditioning are listed in Table 1. The  $UC(x)$  and the parameters for computing the  $CAPEX(x)$  of each equipment were obtained from Turton et al. (2018).

Table 1. Prices of products and raw materials

Process stream	Price	units
$O_2$	155.06	\$/Ton
$N_2$	86.51	\$/Ton
$Ar$	195	\$/Ton
air (pre treatment)	10.0	\$/Ton

Table 2 shows, for each of the eleven decision variables, their respective lower and upper bounds, and the physical units, when it applies. Here,  $T_{E-101/102/103}$  correspond to the outlet hot product temperature of the heat exchangers E-101, E-102 and E-103, respectively.  $Lx_{E1/2}$  are the liquid fraction of the streams entering stages 1 and 28 of the

column T-202, respectively.  $\Delta T_{dew}$  is the hot product temperature rise above the dew point of the stream entering stage 33 of the column T-202.  $F_{cool}$  is the flow rate of the coolant at the compression stage.  $R_{1/2}$  are the ratio of the coolant flows that split before entering the heat exchangers E-101, and E-102, respectively. Since  $R_3$  is defined by the equation  $R_3 = 1 - R_1 - R_2$ , it is not considered as a decision variable.  $P_{C-104}$  is the discharge pressure of C-104, and  $P_{P-101}$  is the discharge pressure of P-101.

Table 2. Upper and lower bounds of the decision variables of the ASU system.

Decision variables	$x^{LB}$	$x^{UB}$	units
$T_{E-101}$	288	303	K
$T_{E-102}$	288	303	K
$T_{E-103}$	288	303	K
$Lx_{E1}$	0.8	1.0	-
$Lx_{E2}$	0.41	0.71	-
$\Delta T_{,dew}$	3.0	5.0	K
$F_{cool}$	4.0	6.0	kmol/s
$R_1$	0.1	0.4	-
$R_2$	0.1	0.4	-
$P_{C-104}$	150	250	kPa
$P_{P-101}$	900	1100	kPa

### 3.2 Evolutionary many-objectives optimization framework

Unlike one-objective optimizations, many-objective optimizations include conflicting objectives. Usually, it is not possible to find a single point capable of optimizing simultaneously all the objective functions. In this sense, a typical approach to solve such problems is to combine all the objectives into a single scalar function by introducing weights. However, the magnitude of these weights depends on an expert opinion in terms of the importance given to each conflicting objective.

As an alternative approach, a set of optimal solutions can be obtained. This set of solutions is referred as the Pareto-optima points, which are non-dominated solutions, meaning that no objective can be improved without penalizing at least another one. The Pareto-optima points delimit the Pareto front (PF), which is a boundary between feasible and infeasible solutions. In this work, the PF is a surface because there are three objectives.

Evolutionary algorithms exhibit suitable properties to obtain reasonable solutions for highly nonlinear problems. The reference vector-guided evolutionary algorithm (RVEA) (Cheng et al., 2016) combines the characteristics required to tackle the proposed many-objective optimization problem. The following description of the algorithm is essentially a summary from Cheng et al. (2016).

The RVEA is guided by a set of predefined reference vectors, which are used to decompose the original optimization problem into single-objective sub-problems for searching a preferred subset of the PF. The partition of the objective space using a set of reference vectors generates several small sub-spaces, while an elitism selection strategy is utilized in each subspace. A *scalarization* approach works as the selection criterion for quantifying the distance from the solutions to the ideal point, and its closeness to the reference vectors. This allows a balance between diversity and convergence. The RVEA has the characteristics of

other decomposition-based approaches when the reference vectors are uniformly generated to cover the whole PF. The definition of a central vector and a radius allow a precise preference articulation of the reference vectors. To obtain a set of uniformly distributed solutions in the objective space, the algorithm uses a strategy for adapting the reference vectors according to the distribution of the candidate solutions. In this sense, the RVEA possesses the ability of approximating the Pareto-optimal solutions specified by the predefined reference vectors when the PF allocates in the whole objective space.

The different steps of the RVEA are summarized in the following algorithm:

**Input:** Given a population size  $N$ , maximum number of generations  $k_{max}$ , a set of unit reference vectors  $V_0 = [V_{0,1}, \dots, V_{0,N}]$

**Output:** Final population  $P_{k_{max}}$

*Initialization:*

Generate the initial population  $P_0$  with  $N$  random individuals

*LOOP Process*

**while**  $k < k_{max}$  **do**

$Q_k \leftarrow$  offspring-creation( $P_k$ )

$P_k \leftarrow P_k \cup Q_k$

$P_{k+1} \leftarrow$  ref.-vector-guided-selection( $k, P_k, V_k$ )

$V_{k+1} \leftarrow$  ref.-vector-adaptation( $k, P_{k+1}, V_k, V_0$ )

$k \leftarrow k + 1$

**end while**

For more details regarding the RVEA algorithm, see Cheng et al. (2016) and the references therein. In our practice, the selected parameters of the optimization algorithm are a population of 88 individuals, 20 generations and 3 iterations in total.

The communication between the Python environment and the commercial process simulator PRO/II takes place through the Python-COM interface (Jones et al., 2019). The Python for Microsoft Windows extensions package known as `pywin32` allows accessing Microsoft Window's Component Object Model (COM) to control other Microsoft applications from Python. Once the communication is established, the PRO/II COM server grants the access to read and write in the objects and streams contained in the process simulation. The ability of manipulating the simulation model permits the iterative evaluation of the high-resolution model in the PRO/II simulator.

The framework for handling the coupling between the PRO/II simulator and the Python environment is depicted in Figure 2. The Python environment contains the many-objective evolutionary optimization algorithm, the conflicting objective functions and the problem constraints. Moreover, the values of the decision variables, set as inputs, are sent through the Python-COM interface to the process simulation in PRO/II. With the provided inputs, the simulation runs. Thereafter, the obtained operating conditions from the simulation return to the Python environment for calculating the optimization objectives.

#### 4. RESULTS

To test the performance of the proposed framework, computational experiments are carried out. The packages

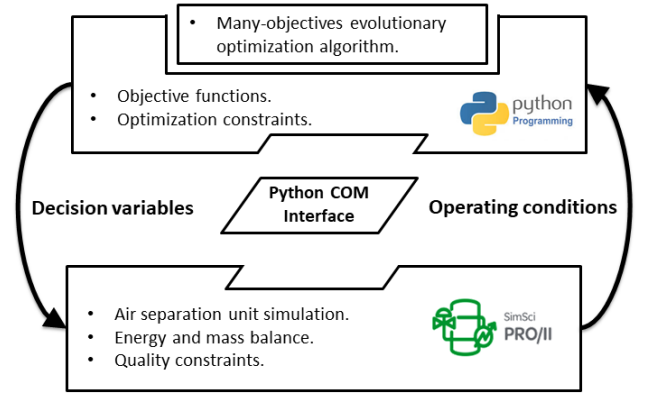


Fig. 2. Framework with the main elements for evolutionary many-objective optimization of an ASU simulation using the coupling of Python and PRO/II simulator.

PRO/II Process Engineering 10.2 (64 bit) and Spyder (Python 3.7) are utilized. We perform the experiments in a laptop PC Intel Core™ i7-8565U CPU @ 1.80GHz with 16.00 GB of installed RAM. In terms of computational time, the evaluation of the first generation takes 0.17 hours (619.14 seconds) and in total the many-objective optimization requires 12.27 hours (44178.35 seconds).

The resultant 3-D relationship of the optimization objectives is portrayed in Figure 3. Here, the colored circles represent the PF, and the smaller grey circles are the remainder obtained feasible solution points. In addition, the blue circles show results that exhibit a positive cash flow while the red circles represent a negative cash flow. This visualization introduces the PF as a surface (colored points) emphasized at a higher cash flow and where the trade-off between the three conflicting objectives can easily be observed.

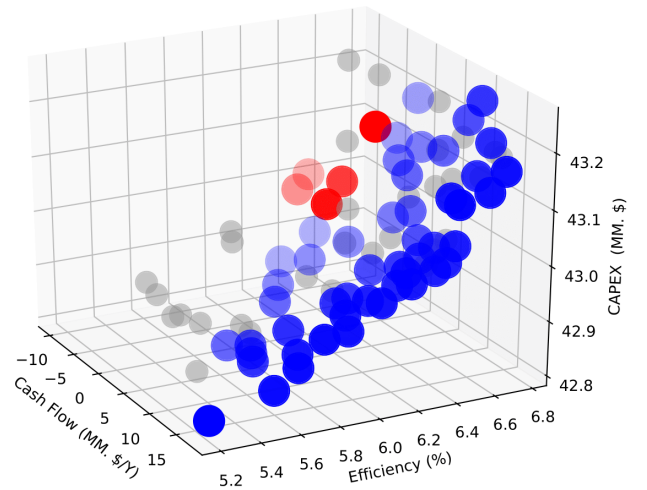


Fig. 3. 3-D solutions. All circles represent feasible solutions. The colored circles correspond to the PF. The red points denote a negative  $CF(x)$ , while the blue points represent a positive  $CF$ .

To facilitate the visualization of the relationship between the objectives, 2-D projections of the results are included in Figure 4. Here, Figure 4 (a) illustrates the  $CAPEX(x)$

vs.  $ef(x)$ . Clearly, the efficiency is directly proportional to the  $CAPEX(x)$ , meaning that at higher capital investments the efficiency of the Rankine Cycle at the compression section increases as well. For further improving the  $ef(x)$  other coolants for the heat exchangers could be evaluated, and a more detailed modelling of the equipment could be performed. Moreover, Figure 4 (b) shows the relationship between the  $CAPEX(x)$  and  $CF(x)$ . At the PF, it is not clear the relationship between the objectives, but those that show a less required capital investment and a higher cash flow appear to be interesting for determining the optimal operational window. Finally, Figure 4 (c) portrays the relationship between the  $ef(x)$  and  $CF(x)$ . Again there is not a clear trend, but the upper east corner contains mainly the PF and shows a higher  $CF(x)$  at good efficiencies of the Rankine cycle. The visualization in different perspectives of the proposed conflicting objectives facilitates the understanding and the influence of such objectives at the PF. These results resemble a good decision-making support-tool for the establishment of a suitable operational window for the ASU.

For analyzing further the set of Pareto-optimal points at the PF and with the objective of establishing an optimal operational window, only the solutions that show a cash flow above 16.0 MM USD per year, an efficiency above 6% and a  $CAPEX(x)$  below 43.0 MM USD are selected for a detailed assessment. Even though the introduced selection is arbitrary, it aims to favor the  $CF(x)$  as a main objective while considering adequate and reasonable values for the other objectives. In this context, the decision-maker will always seek to achieve a good trade-off between all the conflicting objectives. The four selected optimal points along with their objective function values and decision variables are enlisted in Table 3.

Table 3. Selected results allocated at the PF with a cash flow above 16.0 MM USD per year, an efficiency above 6% and a  $CAPEX(x)$  below 43.0 MM USD.

Objectives	Case 1	Case 2	Case 3	Case 4	units
CF	16.28	16.46	17.61	17.66	MM \$/Y
$ef$	6.0	6.2	6.1	6.2	-
$CAPEX$	42.97	42.99	42.97	43.00	MM \$
Variables	Case 1	Case 2	Case 3	Case 4	units
$T_{E-101}$	280.9	280.7	280.5	280.7	K
$T_{E-102}$	302.0	303.0	301.6	303.0	K
$T_{E-103}$	280.8	280.4	280.8	280.6	K
$Lx_{E1}$	1.00	1.00	1.00	1.00	-
$Lx_{E2}$	0.70	0.70	0.71	0.71	-
$\Delta T_{,dew}$	3.32	3.45	3.32	3.24	K
$F_{cool}$	4.36	4.03	4.35	4.03	kmol/s
$R_1$	0.30	0.22	0.30	0.30	-
$R_2$	0.39	0.40	0.39	0.39	-
$P_{C-104}$	161.7	187.4	156.5	189.4	kPa
$P_{P-101}$	1079.8	1027.7	1070.8	1077.9	kPa

Regarding the outlet temperatures of the heat exchangers at the compression section, in all cases, the results are consistent, but different among them. This implies that even though their set-points must be considered independent, its operation should follow the systems' policy. The liquid fractions of the streams entering the column T-202 are consistent as well in all the cases. Moreover, the rise above the dew point shows a very small operational window between (3.24, 3.45) K.

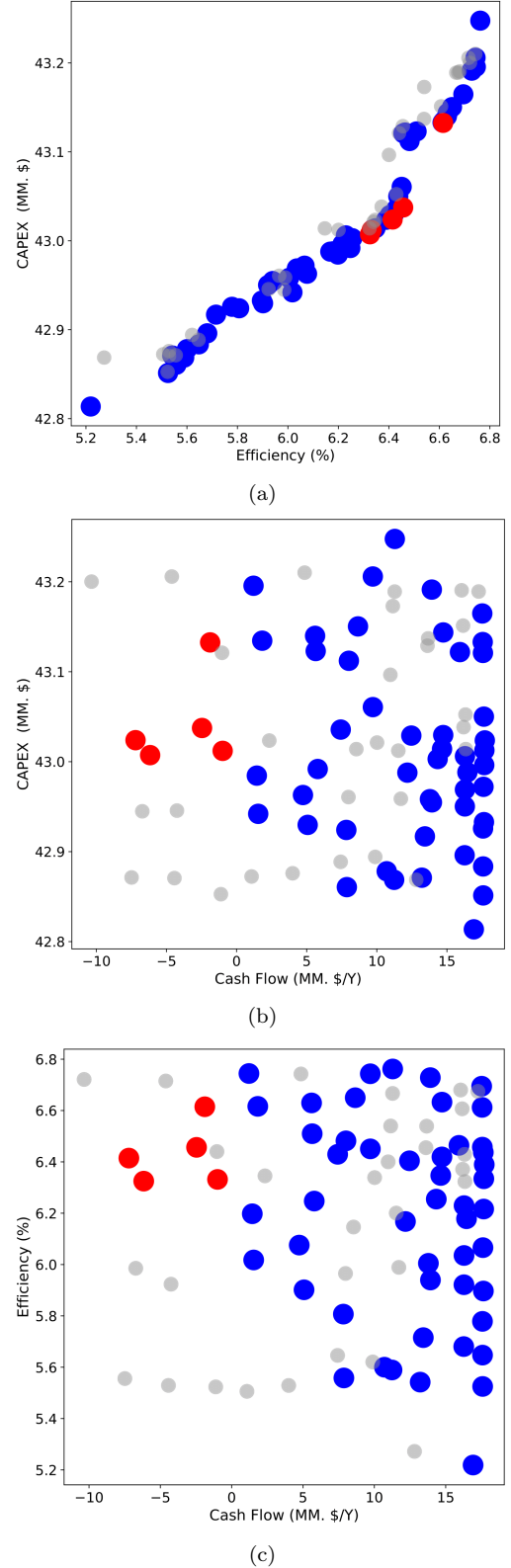


Fig. 4. 2-D projections of the feasible solutions. Colored circles represent the PF. The red points resemble a negative  $CF(x)$ , and the blue points show a positive  $CF(x)$ . Plots labeled as (a), (b) and (c) correspond to the solutions for  $ef(x)$  vs.  $CAPEX(x)$ ,  $CF(x)$  vs.  $CAPEX(x)$ , and  $CF(x)$  vs.  $ef(x)$ , respectively.

The last five decision variables focus on the compression section and the loop that contains the cooling fluid. In this context, the flow rate of the coolant as well as its distribution to the pipelines, before entering the heat exchangers E-101/102/103, shows variability. In terms of  $F_{cool}$ , Case 1 and Case 3 are similar, the same as Case 2 and Case 4, giving an operational window of (4.03, 4.35) kmol/s. Additionally, the ratios for distributing the cooling fluid to the E-101/102/103 show differences. If we choose the highest  $CF(x)$  as a design/operating scenario (Case 4) and its respective  $F_{cool}$ , it would be important to consider the ratios of Case 2 as well because both cases exhibit a similar flow rate. Consequently, to overcome changes in the operation, the selection of an adequate control architecture at the compression section would be beneficial. Finally, the discharge pressure of P-104 shows a range between (156.5, 189.4) kPa, and the discharge pressure of P-101 shows a range between (1027.7, 1079.8) kPa. These results show flexibility in the operation of the ASU and provide guidance on the selection of the equipment required.

## 5. CONCLUSION

In this work, a many-objective optimization framework, coupling the functionalities of Python libraries with the process simulator PRO/II, is implemented and tested for an ASU which focuses on the production of oxygen. The proposed framework is capable of achieving insightful results for establishing a reasonable operational windows for the studied system. In our practice, a simulation-based approach permits the exploration and exploitation of the solution domain towards the construction of a Pareto Front (PF) surface.

A trade-off between objectives is observed in the 3-D visualization of the PF, and the 2-D projections of the results make easier the efforts of decision-makers for reaching final conclusions. Even though in our case study the  $CF(x)$  was favored during the selection, the other two objectives provide important guidance in determining the best results as well. The construction of the PF shows important advantages, especially when compared with other multi or many-objective approaches in which a weighted definition of the objective function is proposed. The selection of such weights depends on an expert opinion and sometimes on trial and error efforts.

Future work in the topic includes the incorporation of uncertainty to the system parameters and variables, the expansion of the  $ef(x)$  objective function and the evaluation of other available many-objective optimization algorithms. Because in our practice the ASU is considered as a whole system (including the compression section), independent studies could provide also a better direction on the proper arrangement of the decision variables. Finally, surrogate based optimization alternatives can be explored to improve the computational time.

## ACKNOWLEDGEMENTS

The authors would like to acknowledge AVEVA for facilitating the process simulator PRO/II 10.2 under the academic program licence for its use at the Polytechnic University of the Coast (ESPOL), Guayaquil, Ecuador,

and to "Corporación Ecuatoriana para el Desarrollo de la Investigación y Academia" (CEDIA) for the financial support given for publishing and presenting this work.

## REFERENCES

- Aneke, M. and Wang, M. (2015). Potential for improving the energy efficiency of cryogenic air separation unit (asu) using binary heat recovery cycles. *Applied Thermal Engineering*, 81, 223–231. doi: 10.1016/j.applthermaleng.2015.02.034.
- Castle, W.F. (2002). Air separation and liquefaction: Recent developments and prospects for the beginning of the new millennium. *International Journal of Refrigeration*, 25(1), 158–172. doi:10.1016/S0140-7007(01)00003-2.
- Cheng, R., Jin, Y., Olhofer, M., and Sendhoff, B. (2016). A reference vector guided evolutionary algorithm for many-objective optimization. *IEEE Transactions on Evolutionary Computation*, 20(5), 773–791.
- Huang, R., Zavala, V.M., and Biegler, L.T. (2009). Advanced step nonlinear model predictive control for air separation units. *Journal of Process Control*, 19(4), 678 – 685. doi: https://doi.org/10.1016/j.jprocont.2008.07.006.
- Jiang, L., Biegler, L.T., and Fox, V.G. (2003). Simulation and optimization of pressure-swing adsorption systems for air separation. *AIChE Journal*, 49. doi: 10.1002/aic.690490508.
- Jones, M.N., Frutiger, J., Ince, N.G., and Sin, G. (2019). The monte carlo driven and machine learning enhanced process simulator. *Computers & Chemical Engineering*, 125, 324–338.
- Manenti, F., Rossi, F., Croce, G., Grottoli, M.G., and Altavilla, M. (2013). Intensifying air separation units. *Chemical Engineering Transactions*, 35.
- Negrellos-Ortiz, I., Flores-Tlacuahuac, A., and Gutiérrez-Limón, M.A. (2018). Dynamic optimization of a cryogenic air separation unit using a derivative-free optimization approach. *Computers & Chemical Engineering*, 109, 1–8.
- Singla, R. and Chowdhury, K. (2019). Comparisons of thermodynamic and economic performances of cryogenic air separation plants designed for external and internal compression of oxygen. *Applied Thermal Engineering*, 160, 114025.
- Tesch, S., Morosuk, T., and Tsatsaronis, G. (2017). Exergetic and economic evaluation of safety-related concepts for the regasification of lng integrated into air separation processes. *Energy*, 141, 2458–2469.
- Turton, R., Shaeiwitz, J.A., Bhattacharyya, D., and Whitling, W.B. (2018). *Analysis, Synthesis, and Design of Chemical Processes*. Pearson Education.
- Whittle, J.S., Pavlov, I., Sacchetti, A.D., Atwood, C., and Rosenberg, M.S. (2020). Respiratory support for adult patients with covid-19. *Journal of the American College of Emergency Physicians Open*, 1(2), 95–101.
- Zhu, G.Y., Henson, M.A., and Megan, L. (2001). Low-order dynamic modeling of cryogenic distillation columns based on nonlinear wave phenomenon. *Separation and Purification Technology*, 24(3), 467 – 487. doi:https://doi.org/10.1016/S1383-5866(01)00147-2.